Charge Fractionalization in a Mesoscopic Ring

Wade DeGottardi,[1] Siddhartha Lal,[1,2] and Smitha Vishveshwara[1]

[1]*Department of Physics, University of Illinois at Urbana-Champaign, 1110 W. Green St., Urbana, Illinois 61801-3080, USA*
[2]*Department of Physical Sciences, IISER-Kolkata, Mohanpur Campus, West Bengal 741252, India*

(Received 18 May 2012; published 8 January 2013)

We study the fractionalization of an electron tunneling into a strongly interacting electronic one-dimensional ring. As a complement to transport measurements in quantum wires connected to leads, we propose noninvasive measures involving the magnetic field profile around the ring to probe this fractionalization. In particular, we show that the magnetic field squared produced by the electron and the power that it would induce in a detector exhibit anisotropic profiles that depend on the degree of fractionalization. We contrast true fractionalization with two other scenarios which could mimic it—quantum superposition and classical probabilistic electron insertion. We show that the proposed field-dependent measures and those of the persistent current can distinguish between these three scenarios.

DOI: 10.1103/PhysRevLett.110.026402 PACS numbers: 71.10.Pm, 03.65.Yz, 73.23.−b, 85.30.Hi

A spectacular feature of strongly correlated low-dimensional electronic systems is that collective behavior renders the electron completely unstable, resulting in its fractionalization [1–8]. As a prime example, in a one-dimensional quantum wire, the Tomonaga-Luttinger liquid (TLL) theory predicts that a momentum-resolved electron tunneling into the wire splinters into charges $(1 \pm g)e/2$ moving in opposite directions, where g, the Luttinger parameter, depends on the ratio of interactions and the Fermi energy and is unity in the absence of interactions [2,4]. Exciting developments in experimental capabilities have enabled the physical realization of such a situation [9]. These studies inspire revisiting fractionalization in a new light and addressing a spectrum of theoretical and physical issues. For instance, can one distinguish true fractionalization from quantum mechanical probabilistic processes? Or even classical probabilities? Are there geometries which could eliminate one of the biggest banes in detecting fractionalization—the effect of leads [2,10–14]? What measurements in such geometries could pinpoint true fractionalization? In this Letter, we answer each of these questions in the context of the ring geometry illustrated in Fig. 1.

Here, an electron tunnels from a lead into a thin mesoscopic ring and, as with the quantum wire [15], has a well-defined momentum profile. Strong interactions within the ring cause an electron associated, for instance, with clockwise Fermi momentum to decompose into two components of charge $(1 \pm g)e/2$ moving in clockwise (CW) and counterclockwise (CCW) directions. Our study focuses on the magnetic field produced by such a situation and the signatures of fractionalization reflected in the spatial distribution of higher moments involving this field. Specifically, we propose measurements of the time-averaged field squared, as for instance can be measured by a superconducting quantum interference device, and the power induced by the field in a pickup loop (see Fig. 1). These measurements have the advantage of purely entailing dc quantities as opposed to high frequency measurements (such as in Ref. [16]) and of constituting weak, i.e., noninvasive, readouts when compared with those involving the attachment of leads.

Fractionalization emerges from the strongly correlated nature of the many-body wave function and is fundamentally different from quantum mechanical superpositions or classical probabilities involving individual particles even though these processes can mimic one another in measurements. To elucidate this point and to distinguish signatures of 'true' fractionalization, we analyze features of the fractionalized state $|F\rangle$ and contrast it to a specific quantum superposition state, $|QS\rangle$, and a classical probabilistic scenario, $\mathbf{M}_\rho$. First, the fractionalized many-body excited state resulting from the tunneling of a CW-moving electron $\psi_+^\dagger(x)$ having a wave function spread $\chi(x)$ above the TLL ground state, $|G\rangle_{LL}$, is given by $|F\rangle = \int \chi(x)\psi_+^\dagger(x)dx|G\rangle_{LL}$ [17]. A quantum superposition state, $|QS\rangle$, that mimics the fractionalized state would consist of superpositions of CW(+)/CCW(−)

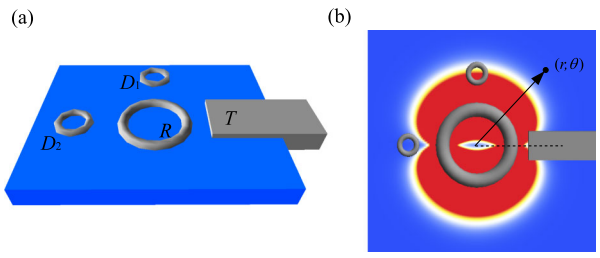

FIG. 1 (color online). (a) Oblique view of the setup in which a clockwise-moving electron injected into the ring from tunnel junction T fractionalizes into clockwise- and counterclockwise-moving quasiparticles. (b) Top-down view of the same setup with an overlay of a spatial plot of $\overline{\langle B^2 \rangle}$ predicted for a ring with Luttinger parameter $g = 0.2$.

electrons excited above a noninteracting Fermi gas ground state $|G\rangle_0$, i.e., $|QS\rangle = \sum_\pm f_\pm \int \chi(x)\psi_\pm^\dagger(x)dx|G\rangle_0$, where $f_\pm = \sqrt{(1 \pm g)/2}$ correspond to the mimicking probabilities. A classical probabilistic situation would correspond to an ensemble of CW and CCW electrons excited in the noninteracting Fermi gas, denoted by the density matrix $\mathbf{M}_\rho = \sum_\pm f_\pm^2 |\pm\rangle\langle\pm|$, where $|\pm\rangle = \int \chi(x)\psi_\pm^\dagger(x)dx|G\rangle_0$. In what follows, after introducing fractionalization in the TLL liquid ring setting, we show that a combination of the two magnetic field measures combined with persistent current signatures in the mesoscopic ring at once distinguish the three different scenarios and provide a means of extracting the Luttinger parameter.

To briefly summarize TLL physics in a ring geometry (see, for example, Ref. [18]), we consider a one-dimensional system with position x denoting the circumferential direction bounded by $0 \le x < 2\pi R$, where R is the radius of the ring. The ring geometry imposes periodic boundary conditions on electron operators such that $\psi(x + 2\pi R) = e^{i2\pi\Phi/\Phi_0}\psi(x)$, where Φ is any flux threading the ring and $\Phi_0 = h/e$. For electrons filling a Fermi sea, we decompose the electron operators as $\psi(x) = \sum_r \psi_r(x)$ where $\psi_r^\dagger$ denotes the creation operator for a $r = \pm$ moving electron. The kinetic energy for linearized low-energy modes moving at a Fermi velocity v_F takes the form $H_0 = -iv_F \int dx \sum_r \psi_r^\dagger \partial_x \psi_r$. As is commonly done, we restrict interaction effects to the short-range form $H_{\rm int} = V \int dx \rho^2(x)$, where $\rho = e\sum_{r=\pm}\rho_r$ is the sum of charge densities $\rho_r = \psi_r^\dagger \psi_r$. Of physical interest, the current operator is given by $\hat{I} = ev_F j$, where $j = \sum_r r\rho_r$.

This model is amenable to a bosonization treatment via the transformation $\psi_r(x) \sim e^{irk_F x}e^{i\sqrt{\pi}\varphi_r(x)}$ giving $\rho_r = k_F/2\pi + r\partial_x\varphi_r/\sqrt{2\pi}$, where the chiral bosonic fields φ_r satisfy the commutation relations $[\varphi_r(x), \varphi_{r'}(x')] = ir\delta_{rr'}\mathrm{sgn}(x - x')$ and k_F is the Fermi momentum. The net Hamiltonian $H_0 + H_{\rm int}$ may be brought into the free TLL form via a Bogoliubov transformation of the ϕ fields [19], yielding

$$H_{LL} = \frac{u}{4}\int dx[(\partial_x\tilde{\varphi}_+)^2 + (\partial_x\tilde{\varphi}_-)^2], \tag{1}$$

where $u = v_F/g$ is the the plasmon velocity, g is the Luttinger parameter with $g \equiv 1/\sqrt{1 + 2V/\pi\hbar v_F}$, and $\tilde{\varphi}_\pm(x \mp ut)$ are transformed chiral bosons.

The fractionalization of an electron can be seen by representing an electron operator having CW Fermi momentum in terms of the chiral bosons:

$$\psi_+^\dagger(x,t) \sim e^{-ik_F x}e^{-i\frac{\sqrt{\pi}}{2\sqrt{g}}[(1+g)\tilde{\varphi}_+(x,t)+(1-g)\tilde{\varphi}_-(x,t)]}. \tag{2}$$

By relating the chiral bosonic fields to the charge and current density operators, ρ and j, respectively, it follows that the operator $e^{-i\sqrt{\frac{\pi}{g}}\tilde{\varphi}_+(x,0)}$ creates a unit charge e that at time t can be found at position $x - ut$. Thus, we see that the electron operator in Eq. (2) creates the fractional charges $(1 \pm g)e/2$ moving in opposite directions. More explicitly, in the situation of interest, the state of the ring after the injection of a CW-moving electron at time $t = 0$ is given by $|F\rangle = \int \chi(x)\psi_+^\dagger(x, t = 0)dx|G\rangle_{LL}$ [5]. It is straightforward to calculate the expectation value of the current in this state, $I(x,t) = \langle\hat{I}\rangle_F \equiv \langle F|\hat{I}(x,t)|F\rangle$, yielding

$$I(x,t) = \frac{eu}{4\pi R}[(1+g)|\chi(x-ut)|^2 + (1-g)|\chi(x+ut)|^2]. \tag{3}$$

The form of the current explicitly demonstrates that the electron splinters into two components that rotate in opposite directions, have the same profile $\chi(x)$, and carry charges $(1 \pm g)e/2$.

The magnetic field produced by these counterpropagating charges can be evaluated by using the Biot-Savart law to define the magnetic field operator at position $\mathbf{r}$ as $\hat{\mathbf{B}} = \frac{\mu_0}{4\pi}\int d\ell\,\hat{\mathbf{I}}(\ell) \times \mathbf{r}/|\mathbf{r}|^3$, where μ_0 is the permeability of free space. At any given point having polar coordinates (r, θ) in the plane of the ring, where the origin is at the ring's center and the electron is inserted at $(R, 0)$, the current in Eq. (3) produces a field perpendicular to the plane. For the case of χ having a spread much smaller than the ring diameter, the z component of the field takes the form

$$\langle\hat{B}_z\rangle_F = \frac{\mu_0 e\omega}{2R}[(1+g)h(t) - (1-g)h(-t)], \tag{4}$$

where $\omega = u/R$ and $h(t) = [1 - a(t)]/[\frac{r^2}{R^2} - 2a(t) + 1]^{3/2}$, $a(t) = r\cos(\omega t - \theta)/R$. In principle, a time-resolved measurement of the magnetic field, as with other quantities, such as the conductance, would yield information on fractionalization. However, as is the goal here, we seek low-frequency or time-averaged signatures. Although the tunneling of the electron picks out a specific point on the ring, signatures are effaced by time averaging any quantity that is linear in the ring current. For example, $\overline{\langle B_z\rangle}$ shows an isotropic spatial profile. [Here, we use $\langle\cdot\rangle$ to denote time-dependent quantum mechanical or statistical expectation values of the specific state in question and an overline $\bar{\cdot}$ for a long ($\gg\omega^{-1}$) time average.]

We thus focus on two measures that are quadratic in the current and can be obtained from a continuous weak linear measurement [20] via inductive coupling to the ring. The first is simply $S(r,\theta) = \overline{\langle B_z^2\rangle}$, which can be accessed in a superconducting quantum interference device detector biased to a minimum of its I-V characteristic curve. The second is the average power received by a detector, for example, an ultrasensitive bolometer. For a small conducting detector (ignoring local spatial variations in the magnetic field), this is given by $P(r,\theta) = \overline{\langle\partial_t B_z\rangle^2}$. Crucially, note that the former involves a quantum average of a quadratic operator and the latter that of a linear operator.

The forms of the moments S and P can be easily evaluated by taking appropriate quantum expectations ($\langle\rangle$) and time averages (overline) to obtain $S(r,\theta) = (\frac{\mu_0 e\omega}{2R})^2[(1+g^2)\overline{h^2(t)} - (1-g^2)\overline{h(t)h(-t)}]$ and a similar form for $\tilde{P} \equiv P/\omega^2$ with $h(t)$ replaced by its time derivative $h'(t)$. Information on fractionalization is best analyzed by resolving these quantities into their angular Fourier coefficients:

$$S/\tilde{P}(r,\theta) = \left(\frac{\mu_0 e\omega}{2R}\right)^2 \sum_{m=0}^{\infty} A_m^{S/P}(r)\cos 2m\theta. \qquad (5)$$

In the noninteracting ($g = 1$) limit, an electron circles the ring in the CW direction, retaining rotational symmetry on average and thus we have $A_m^{S/P} = 0$, $m \neq 0$.

The plots in Fig. 2 capture our central result that higher moments of the current and of the magnetic field profile (in our case, S and P) reflect the concurrent motion of fractionalized charge components in their rotational symmetry broken distributions. In the explicit forms of S and P above, given that $\overline{h^2(t)}$ preserves rotational symmetry while $\overline{h(t)h(-t)}$ breaks it, we see that primarily $A_0^{S/P}$ scale as $1+g^2$ and $A_{m\neq 0}^{S/P}$ as $1-g^2$. This distribution is illustrated in the plots of Fig. 2 and also agrees with the rotationally symmetric noninteracting limit ($g = 1$) [21]. The bilateral symmetry of the plots reflects the two charge components moving away from the injection point and towards the diametrically opposite point. That these two special points exist for any arbitrary closed shape suggests that our result that fractionalization causes a distribution that distinguishes two points is robust for any closed loop.

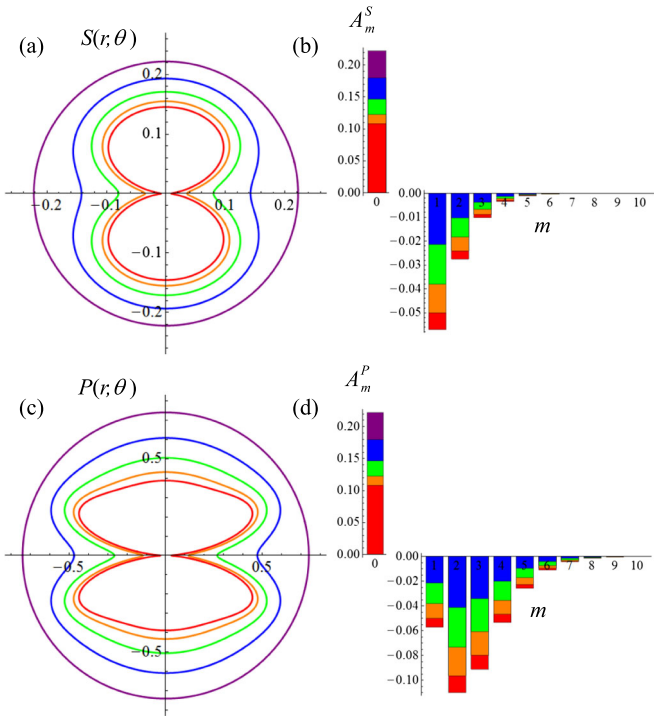

FIG. 2 (color online). Polar plots of (a) $S(r,\theta) = \overline{\langle B_z^2(t)\rangle}$ and (b) $P(r,\theta) = \overline{\langle \partial_t B_z(t)\rangle^2}$ at $r = 2R$ for values of the Luttinger parameter $g = 1.0, 0.8, 0.6, 0.4, 0.2$ (from outermost and most isotropic to the innermost) as a function of θ. Bar graphs of the spectral weight of the maps (c) S and (d) P showing the even Fourier coefficients as defined in Eq. (5), i.e., the height of columns for $m = 0, 1, 2$ correspond to the zeroth, $\cos 2\theta$, and $\cos 4\theta$ terms, respectively (the zeroth and nonzeroth coefficients are shown on a different scale). With increasing fractionalization (decreasing g), spectral weight is transferred to the nonzeroth coefficients reflecting increasing anisotropy.

We contrast the behavior of the moments S and P in the fractionalized state to the quantum and classical probabilistic situations. In the quantum state $|QS\rangle$, a superposition of CW- and CCW-moving electrons, quantum averages of operators that are linear in the current mimic charge fractionalization while higher moments (for example, $\langle \hat{B}_z^2\rangle$) of linear operators do not. Thus, $S = \overline{\langle \hat{B}_z^2\rangle}$ is isotropic but $P = \overline{\langle \partial_t \hat{B}_z\rangle^2}$ shows an anisotropic profile similar to that of Fig. 2(b). For the classical situation described by the density matrix $\mathbf{M}_\rho$, the moments are evaluated by separately considering CW and CCW electrons and adding their appropriately weighted contributions. Thus, both moments yield isotropic profiles. As summarized in Table I, the two measurements therefore can distinguish between the three possible scenarios.

In addition to the differences mentioned here, Ref. [5] distinguishes true fractionalization from other situations by the profound observation that charge fluctuations are in fact a feature of the many-body ground state and the background of particle-hole excitations while the fractionalized electron is itself 'sharp.' Translated to our setting, we expect fluctuations in the magnetic field to be induced even by the quiescent TLL ring (having no extra tunneled electron) and identical to those induced by the fractionalized state $|F\rangle$.

Thus far, we have described the injection localized electron wave packet as a superposition of plasmon-like modes described by Eq. (1). Due to coupling to the environment [22–24] and quasiparticle interactions due to anharmonic effects [15], these modes have a finite lifetime,

TABLE I. Results of various measurements exemplifying how fractionalization ($|F\rangle$) in a TLL can be differentiated from the quantum ($|QS\rangle$) and classical scenarios ($\mathbf{M}_\rho$) considered in the text. Time-averaged quantities S and P can display isotropic (I) or anisotropic (AI) distributions. Persistent current measurements can yield nonvariable (NV) or variable (V) outcomes for repeated measurements.

	$\|F\rangle$	$\|QS\rangle$	$\mathbf{M}_\rho$
$S(r,\theta) = \langle \hat{B}_z^2\rangle$	AI	I	I
$P(r,\theta) = \langle \partial_t \hat{B}_z\rangle^2$	AI	AI	I
Persistent Current	NV	V	V

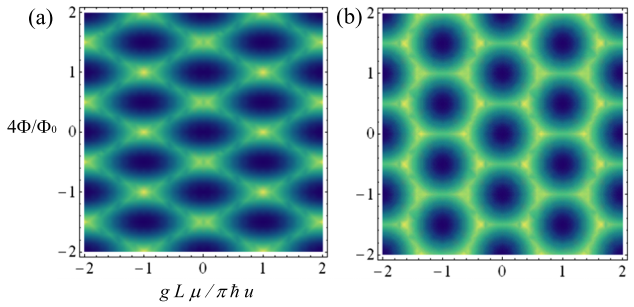

FIG. 3 (color online). Ground state structure obtained from the Hamiltonian H_{NJ} of Eq. (6). Each cell corresponds to a given electron number (N) and persistent current (J) which optimizes H_{NJ} as a function of chemical potential (horizontal axis) and magnetic flux (vertical); bright lines indicate a transition in which J or N change by 1. Cells are (a) diamond shaped for $g = 1$ (noninteracting system) and (b) hexagonal shaped for $g\ (= 1/2) \neq 1$ with horizontal side length $1 - g^2$.

giving rise to a characteristic decoherence time τ_d within which measurements need to be performed. However, for time scales longer than τ_d, no plasmons are excited and tunneled electrons need purely be described by the excess electron number, $N = \sum_r n_r$, and the persistent current due to the number imbalance between CCW- and CW-moving electrons, $J = \sum_r r n_r$, where we define $n_r = r\Phi/\Phi_0 + \int dx \rho_r$. The optimal values of these 'topological' quantities N and J can be tuned by the application of a gate potential μ and external flux Φ, and can be determined by minimizing the energy functional derived from Eq. (1) [25]

$$H_{NJ} = \frac{\pi\hbar u}{4\pi R}\left[\frac{1}{g}N^2 + g\left(J + \frac{2\Phi}{\Phi_0}\right)^2\right] - \mu N. \qquad (6)$$

The regions of different optimal N and J values can be charted by Coulomb blockade measurements wherein conductance peaks track electron occupation numbers on the ring. We show the boundaries for these regions in (dimensionless) μ-Φ parameter space in Fig. 3. Interactions render these regions to be generically hexagonal, characterized by horizontal sides of length $1 - g^2$. Thus, the geometry of this diagram is an easily accessible, alternate means of extracting g, the Luttinger parameter.

A highlight of this slow-time regime is that it offers another route to distinguishing the fractionalized state $|F\rangle$ by way of persistent current analysis. Ultimately this state is associated with a CW electron and hence has the fixed current value $J = +1$ while the quantum and classical states characterized by $|QS\rangle$ and $\mathbf{M}_\rho$ involve CW and CCW electrons, thus showing values $J = \pm 1$ which vary between measurements. Thus, as summarized in Table I, the anisotropy in moment S and nonvariability in persistent current distinguish the fractionalized state from the quantum and classical scenarios (though the latter is not a smoking gun test) while anisotropy in the moment P distinguishes the classical scenario.

Finally, turning to actual experiments, the ring geometry can be achieved in the same fashion as in situations that have hitherto measured persistent currents [26], Aharonov-Bohm oscillations, or ring-based Kondo physics [27]. To provide relevant physical estimates, for radius $R \approx 1\ \mu$m and a typical circulating frequency $\omega \approx 10^{11}$ Hz, we have $(\mu_0 e\omega/2R)^2 \approx (0.1\ \text{milligauss})^2$ and $(\mu_0 e\omega^2/2R)^2 \approx (80\ \text{T/sec})^2$. An important requirement is that the injection of an electron must be made on a time scale $\tau_T \ll 1/\omega$ in order for there to be a 'clean' injection of the electron. For the ring, we have $\tau_T = R_T C$ where R_T is the tunnel junction resistance and C ($\sim \epsilon_0 R \sim 10^{-17}$ F) is the ring capacitance. This gives the requirement that $R_T \ll 1$ MΩ. On the other hand, the Coulomb blockade limit holds only if $R_T \gg \frac{h}{e^2} = 26$ kΩ. Thus, we need $R_T \sim 100$ kΩ. Another consideration is that interaction effects at the tunneling point restrict the energy window in which our results hold [22]. The role of the electron's spin can also come into play and can be analyzed by a simple generalization of our results.

In conclusion, we have presented an alternative to the quantum wire based electron-in electron-out paradigm for charge fractionalization in the arena of weak measurements in mesoscopic rings. Our envisioned setup discerns subtle attributes that distinguish fractionalization from quantum and classical probabilistic scenarios and is within the reach of current nanotechnology.

We are grateful to Raffi Budakian and Charles Kane for their perceptive comments. For their support, we thank the NSF under Grant No. DMR 0644022-CAR (W. D. and S. V.), the Simons Foundation (Grant No. 229047 to S. V.) and the DST, Govt. of India, under a Ramanujan Fellowship (S. L.).

[1] V. V. Deshpande, M. Bockrath, L. I. Glazman, and A. Yacoby, Nature (London) **464**, 209 (2010).
[2] I. Safi and H. J. Schulz, Phys. Rev. B **52**, R17040 (1995).
[3] I. Safi, Ann. Phys. (Paris) **22**, 463 (1997).
[4] K.-V. Pham, M. Gabay, and P. Lederer, Phys. Rev. B **61**, 16 397 (2000).
[5] J. M. Leinaas, M. Horsdal, and T. H. Hansson, Phys. Rev. B **80**, 115327 (2009).
[6] M. Horsdal, M. Rypestøl, T. Hansson, and J. M. Leinaas, Phys. Rev. B **84**, 115313 (2011).
[7] K. Le Hur, Phys. Rev. B **74**, 165104 (2006); Phys. Rev. Lett. **95**, 076801 (2005).
[8] I. Garate and K. Le Hur, Phys. Rev. B **85**, 195465 (2012).
[9] H. Steinberg, G. Barak, A. Yacoby, L. N. Pfeiffer, K. W. West, B. I. Halperin, and K. Le Hur, Nat. Phys. **4**, 116 (2007).
[10] D. L. Maslov and M. Stone, Phys. Rev. B **52**, R5539 (1995).
[11] V. V. Ponomarenko, Phys. Rev. B **54**, 10 328 (1996).
[12] I. Safi, arXiv:0906.2363.
[13] S. Pugnetti, F. Dolcini, D. Bercioux, and H. Grabert, Phys. Rev. B **79**, 035121 (2009).

[14] J. U. Kim, W.-R. Lee, H.-W. Lee, H.-S. Sim, Phys. Rev. Lett. **102**, 076401 (2009).
[15] K. Le Hur, B. I. Halperin, and A. Yacoby, Ann. Phys. (N.Y.) **323**, 3037 (2008).
[16] B. Trauzettel, I. Safi, F. Dolcini, and H. Grabert, Phys. Rev. Lett. **92**, 226405 (2004).
[17] As will become clear later in the text, the tunneling of a CCW electron $|F'\rangle = \int \chi(x)\psi_{\perp}^{\dagger}(x)dx|G\rangle_{LL}$ results in the same signal (see Fig. 1).
[18] D. Loss, Phys. Rev. Lett. **69**, 343 (1992).
[19] M. Stone, *Bosonization* (World Scientific, Singapore, 1994).
[20] D. V. Averin, Physica (Amsterdam) **352C**, 120 (2001).
[21] In the case of P measured using bolometers, an important experimental consideration is the heat which may flow from the ring to the substrate. This heat flow could obscure the 'signal' which involves the difference between the heat dissipated in detectors D_1 and D_2 (see Fig. 1). Such an effect may be minimized by the selection of a substrate with low thermal conductivity and/or trenches which prevent the flow of phonons between the ring and the detectors.
[22] I. Safi and H. Saleur, Phys. Rev. Lett. **93**, 126602 (2004).
[23] A. H. Castro Neto, C. de C. Chamon, and C. Nayak, Phys. Rev. Lett. **79**, 4629 (1997).
[24] P. Cedraschi, V. V. Ponomarenko, and M. Buttiker, Phys. Rev. Lett. **84**, 346 (2000).
[25] J. M. Kinaret, M. Jonson, R. I. Shekhter, and S. Eggert, Phys. Rev. B **57**, 3777 (1998).
[26] A. C. Bleszynski-Jayich, W. E. Shanks, B. R. Ilic, and J. G. E. Harris, J. Vac. Sci. Technol. B **26**, 1412 (2008).
[27] See, for example, U. F. Keyser, C. Fühner, S. Borck, R. J. Haug, M. Bichler, G. Abstreiter, and W. Wegscheider, Phys. Rev. Lett. **90**, 196601 (2003).